Influence of Regional Climate on Aerodynamic Forces for Long-Span Bridge Deck

Sourav Ghosh[1][0009-0006-2629-8409], Puja Halder[2], and Abhishek Hazra[3][0000-0003-0326-4151]

[1]Narula Institute of Technology, 81, Nilgunj Rd, Jagarata Pally, Deshpriya Nagar, Agarpara, Kolkata, West Bengal 700109, India, souravghosh.jeet@gmail.com

[2]Sanaka Educational Trust's Group of Institutions, Malandighi, Durgapur, West Bengal 713212, puja.mbc11@gmail.com

[3]Narula Institute of Technology, 81, Nilgunj Rd, Jagarata Pally, Deshpriya Nagar, Agarpara, Kolkata, West Bengal 700109, India, abhishek.hazra@nit.ac.in

Abstract

This study frames the aerodynamic response of the reinforced concrete trapezoidal box grider under extreme climatic conditions from three geographically distinct regions: the katabatic wind-dominated Antarctic, the transitional Arctic Circle, and the hot, low-density Sahara Desert, highlighting the micro parameters of the climate influencing the aerodynamic response. Computational fluid dynamics (CFD) simulation was done in ANSYS Fluent, addressing the utilisation of the standard k-ε turbulence model and Sutherland's temperature-dependent viscosity formulation. Aerodynamic coefficients were evaluated from -8° to +8°. The validation against the literature amplifies the accuracy of the methodology. The results indicate the vital role of climatic parameters on aerodynamic force. The cold & high wind speed as from Antarctica shows the most critical aerodynamic response with a stronger eddy viscosity; in contrast, the Sahara desert's hot and low-density atmosphere provided a low substantial force The findings highlight that aerodynamic force magnitudes vary greatly with regional climatic parameters, indicating that design considerations must incorporate localised environmental factors to ensure bridge safety and performance under extreme wind conditions. This study provides novel insights into region-specific aero-dynamic challenges for long-span bridge decks, promoting better-informed structural design to mitigate risks associated with diverse climatic influences.

Keywords: Aerodynamic, Eddy viscosity, regional wind effect, Sutherland's formula

1 Introduction

In this realm of civil engineering, developing long-span bridges is one of the significant evolutions. This infrastructure enables efficient transportation across geographical barriers such as valleys, rivers, and straits. The growth of population and urbanisation has intensified, and the demand for longer, sustainable, and aesthetically refined bridge structures has increased. With the demand for advancement in infrastructural revolution, there come a lot of challenges for ensuring that the structure shall not only withstand the static load but also shall deal with the complex dynamic loading under different environmental factors, especially for the induced wind influenced by the climate [1]. The study of by Montaya et al. 2021, support the statement, where he has conducted a analytical simulation to identify the aerodynamic performance of twin-box bridge decks, which represents as the critical research area, particularly due to the complex interaction of gap distance, as well as deck geometry, and

aeroelastic phenomena like flutter and buffeting, he additionally joined the fragmented pieces of previous studies on aerodynamic responses, which emphasizes the sensitivity of aerodynamic responses to the gap-to-depth ratio, identifying thresh-olds beyond which flow patterns and vortex dynamics shift significantly [2]. Their integration into long-span bridge design remains recent. Along with that, the implementation of an economical design for a long-span bridge used in a steel twin box girder (STBG) without any appendages. Along with that, the gap distance in the twin box girder influences the buffeting effect that is evident in the previous studies [3]. Rather than that, limited research was conducted to include all the parameters for amplifying STBG capability and nullifying its loopholes. Nevertheless, very few parametric analyses were conducted throughout the aerodynamic context, where a parametric buffeting analysis of long-span railway bridges confirmed that skewed wind directions substantially affect buffeting loads on train-bridge systems, impacting structural fatigue and ride comfort [4, 5]. Additionally, recent studies highlight the wind power generation from the measurable climatic impact, including localised nighttime warming, by reassignment of heat and altering boundary layer mixing [6]. Moreover, climate change driven by wind pattern shifts in North America altered design wind speeds and structural reliability, which may impact the energy production, grid resilience, and necessitate revised safety margins for bridge and infrastructure design [7]. The scrutinised outcome indicates the lack of investigation with respect to climatic parameters; in contrast, they have focused on macro parameters of the wind.

This article focuses on analysing the dynamic response of the bridge deck under extreme conditions, along with diversified climatic parameters. Throughout the analysis, several parameters of the climate were considered, such as wind speed, angle of at-tack, turbulence percentage, dynamic viscosity, and temperature. All these parameters were integrated using Sutherland's formula, along with the standard k-ε turbulence model, which was employed for the modelling of air as well as to simulate the enhanced response of the deck. ANSYS Fluent was used throughout the analysis.

2 Methodology

The study elaborates that the total aerodynamic (F_{DT}) acting on the bridge deck is decomposed into different components, pressure drag force (F_{DP}) and frictional drag force (F_{DF}) acting upon the bridge deck. In this section, we can understand that the drag force (F_D) and moments (M) are easy to compute by numerical simulation. Those forces are used to analyse the lift force coefficient (C_L), drag force coefficient (C_D), and moment coefficient (C_M). Fig.4 mentions the different components of force, where (F_H) is the horizontal force, (F_V) is the vertical force, (F_D) is the drag force, (F_L) is the lift force, M is the moment, and α is the angle of attack. [8], The equation 1 below defines the total force (F_{DT}) applied on the deck is the sum of pressure drag force (F_{DP}) and frictional drag force (F_{DF}), which can be further break into equation 2, 3 & 4 where the abbreviation denotes the following symbols, pressure drag coefficient concerning angle of attack ($C_{DP}(\alpha)$), frictional drag coefficient concerning angle of attack ($C_{DF}(\alpha)$), depth of the deck D, span of the bridge is L, breath of deck B, drag coefficient concerning the angle of attack $C_D(\alpha)$, tributary length (ΔLi), mean pressure (pi), shear stress along the direction of drag force (six), overall monitoring points (n), moni-toring point (i), and the angle between the vertical axis and pressure direction (Hi). Finally, by simplifying the equations, we get the formula of $C_D(\alpha)$, $C_{DP}(\alpha)$, $C_L(\alpha)$, and $C_M(\alpha)$ mentioned in equations 5, 6, 7, and 8. The equations of forces are simplified below with a schematic diagram in Fig. 1

$$F_{DT} = F_{DP} + F_{DF} = 0.5\rho U^2 C_{DP}(\alpha) D_L + 0.5\rho U^2 C_{DF}(\alpha) D_L \quad (1)$$

$$F_{DT} = 0.5U^2 C_D(\alpha) D_L \quad (2)$$

$$F_{DT} = \sum_i^n = 1 p_i \Delta L_i \sin\theta_i \quad (3)$$

$$F_{DF} = \sum_i^n = 1 \tau_{iX} \Delta L_i \quad (4)$$

$$C_D(\alpha) = \frac{F_{DT}}{0.5\rho U^2 D_L} \quad (5)$$

$$C_{DP}(\alpha) = \frac{F_{DP}}{0.5\rho U^2 D_L} \quad (6)$$

$$C_L(\alpha) = \frac{F_L}{0.5\rho U^2 B_L} \quad (7)$$

$$C_M(\alpha) = \frac{M}{0.5\rho U^2 B_L} \quad (8)$$

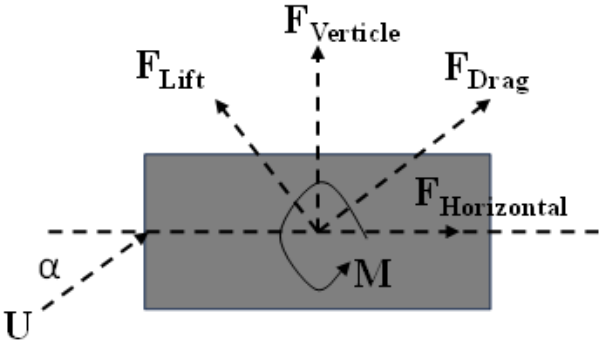

Fig. 1. Aerodynamic Forces diagram (P. Haldar & S. Karmakar (2023)

2.1 Validation

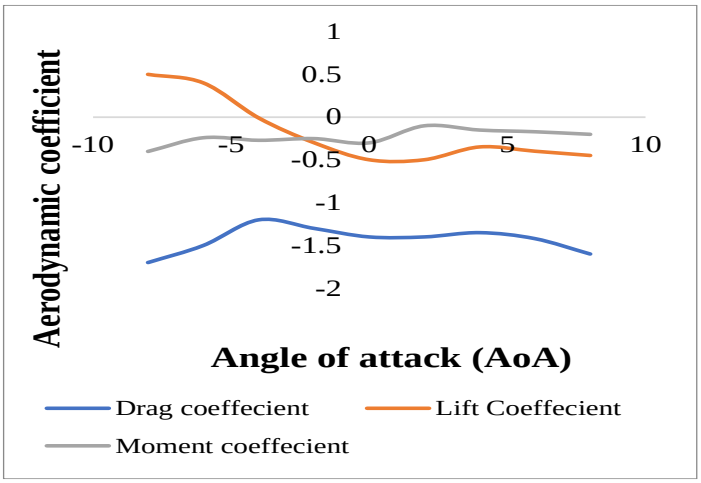

Fig. 2. Plot of Aerodynamic Coefficients (P. Haldar & S. Karmakar, 2023)

This article was chosen for validation because the framework of this piece was vali-dated against the experimental results of the bridge deck. The validation of the RC deck was done by comparing the analytical results with the results obtained from P. Haldar & S. Karmakar, 2023 [8]. The results of C_D, C_L, and C_M have come close enough at different angles of attack. The

analysis was done in ANSYS Fluent. The magnitude of the results matches the reference given below in Fig. 3.

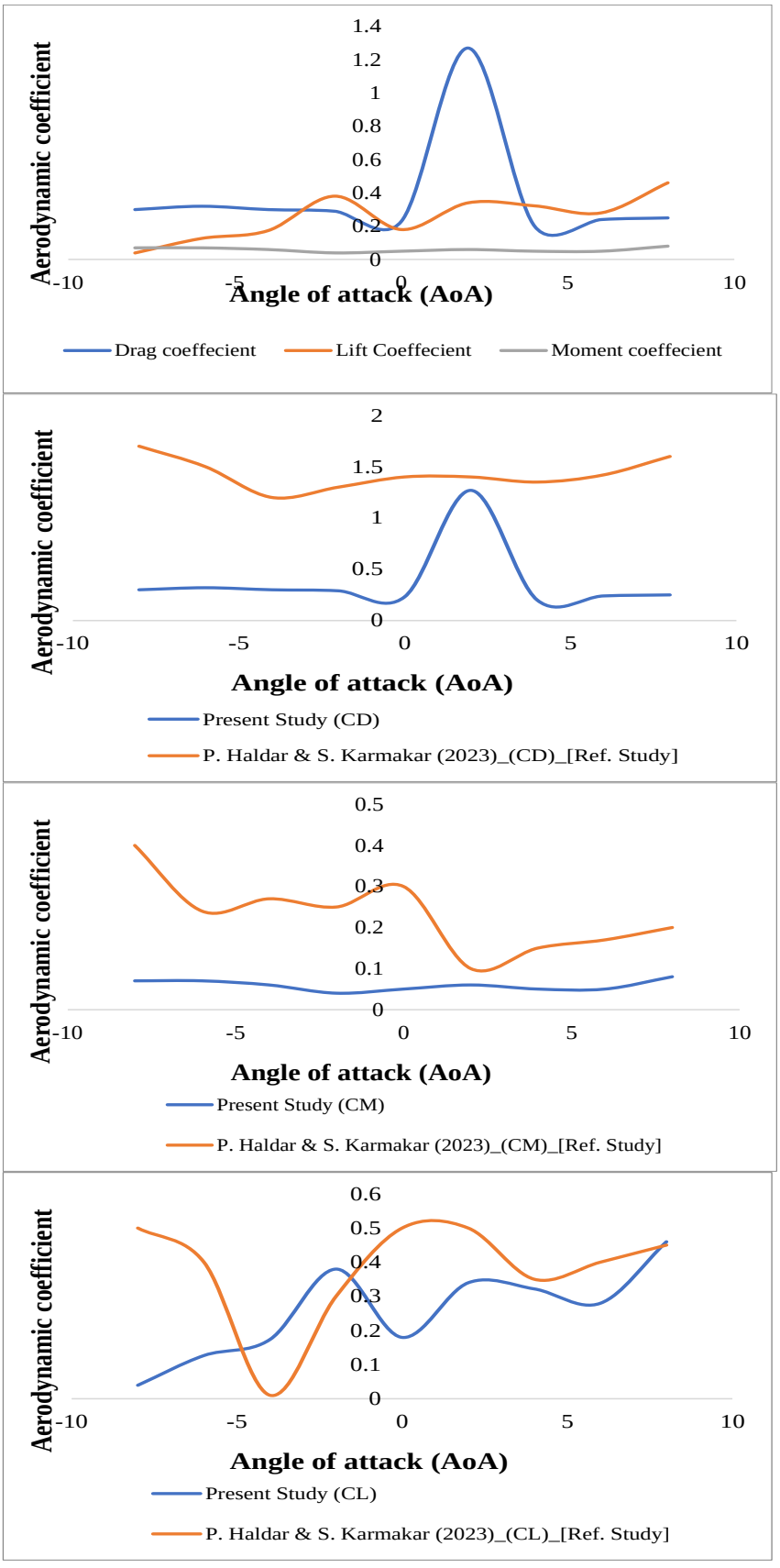

Fig. 3. Comparison of the magnitude of aerodynamic coefficients (C_D, C_L, C_M)

2.2 The governing equations used throughout the model for analysis

The standard k-ε model was utilised due to its balanced computational efficiency and proven reliability in turbulent flow simulations. The advanced model like RNG, realizable k-ε, and LES, provides perfect accuracy for unsteady flows. The computational cost and complexity are higher in this realm of aerodynamics. Therefore, there might be a chance of proclamation in future for sensitivity tests with these models to further validate results.

The k-ε numerical model is trending equations in the field of aerodynamics in ANSYS Fluent. It estimates the turbulent kinetic energy (k) and its dissipation rate (ε) developed by Launder and Spalding. It combines theory and experiments to give reliable and cost-effective results for turbulent flow, even though ε is based on empirical data. The equation of k is directly derived from the original form of the Navier-Stokes equations mentioned in eqn. (9). However, the equation for ε is not derived mathematically, but rather developed using physical intuition and empirical adjustments, and it does not closely resemble the exact mathematical formulation mentioned in eqn. (10) [9]. The standard k-ε model postulates the turbulent flow, neglecting molecular viscosity, making it unsuitable for transitional regimes. To address its limitations and improve accuracy across varied flow conditions, enhanced variants were developed by the researchers, such as the RNG and k-ε models, both of which are available in ANSYS Fluent for broader applicability.

RNG k-ε Model [10]: According to the Renormalisation Group (RNG) theory, the model includes additional terms that improve the flow's accuracy for high strain rates, swirling flows, and transitional regimes.

Realisable k-ε Model [10]: This version ensures that the model adheres to certain physical constraints (realisability conditions), improving predictions for boundary layer flows, separation, and recirculation zones.

Kinetic energy (k) equation:

$$\left(\frac{\partial(\rho K)}{\partial t}\right)+\left(\frac{\partial(\rho K U_i)}{\partial x_i}\right)=\frac{\partial}{\partial x_i}\left[\left(\frac{\mu+\mu t}{\sigma k}\right)\frac{\partial k}{\partial x_j}\right]+G_k+G_b+\rho\epsilon-Y_M+S_k \qquad (9)$$

Turbulent dissipation rate (ε) equation:

$$\left(\frac{\partial(\rho\varepsilon)}{\partial t}\right)+\left(\frac{\partial(\rho\varepsilon U_i)}{\partial x_i}\right)=\frac{\partial}{\partial x_j}\left[\left(\mu+\frac{\mu t}{\sigma\varepsilon}\right)\frac{\partial\varepsilon}{\partial x_j}\right]+G_{1\varepsilon}\left(\frac{\varepsilon}{k}\right)(G_k+C_{3\varepsilon}G_b)-C_{2\varepsilon}\rho\frac{\varepsilon^2}{k}+S_\varepsilon \quad (10)$$

ρ: fluid density

U_i: velocity component in the i-th direction

μ: dynamic viscosity

μ_t: eddy viscosity

σ_k, σ_ε: turbulent Prandtl numbers for k and ε

G_k: generation of turbulence kinetic energy due to mean velocity gradients

G_b: generation of turbulence kinetic energy due to buoyancy

Y_M: Contribution of fluctuating dilatation in compressible turbulence to the overall dissipation rate

S_k, S_ε: user-defined source terms

$C_{1\varepsilon}$, $C_{2\varepsilon}$, $C_{3\varepsilon}$: model constants

The turbulent (eddy) viscosity is modelled as:

$$\mu_t = \rho C_\mu \left(\frac{k^2}{\varepsilon}\right) \quad (11)$$

The following standard model constants are:

C_μ=0.09, σ_k=1, σ_ε=1.3, $C_{1\varepsilon}$=1.44, $C_{2\varepsilon}$=1.92

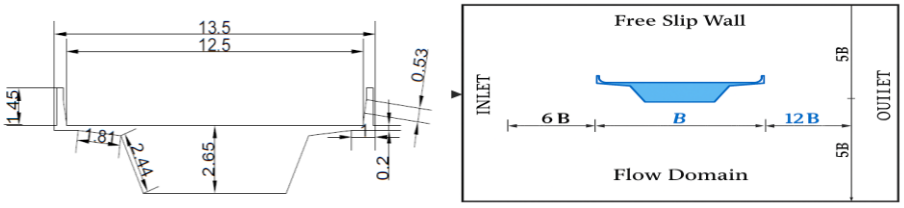

Fig. 4. Dimension of Deck and flow domain.

2.3 Air modelling & climatic conditions

The air pressure was designed according to Sutherland's formula. A temperature-dependent model is used to calculate the dynamic viscosity of gases more accurately than using a constant value. The equation is represented as:

$$\mu(T) = \mu_0 \left(\frac{T}{T_0}\right)^{\frac{3}{2}} \times \left[\frac{(T_0+S)}{(T+S)}\right] \quad (12)$$

μ(T): Dynamic viscosity at temperature T

μ_o: Reference viscosity at reference temperature T_o

T: Local temperature (in Kelvin)

T_o: Reference temperature

S: Sutherland constant (for air: ~110.4 K)

Table 1. Climatic conditions considered for the analysis and their reference

Nation	Density (Kg/m^3)	Wind speed (m/s)	Dynamic viscosity (Kg/ms)	Temp (°C)	Turbulence (%)	Ref
Antarctic	1.225	90.8	1.81E-05	-89	80	[11]
Arctic Circle	1.6	5.5	1.71E-05	0	50	[12]
Sahara Desert	1.204	3	1.81E-05	47	60	[13]

3 Results and discussions

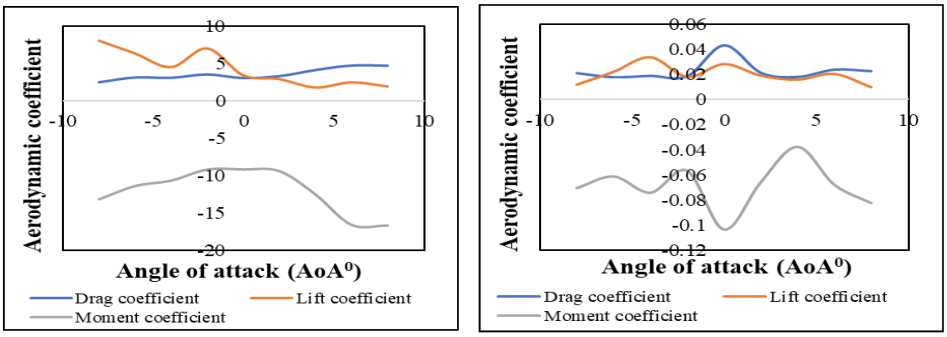

a) Katabatic wind-prone Antarctic region

b) Arctic Circle region

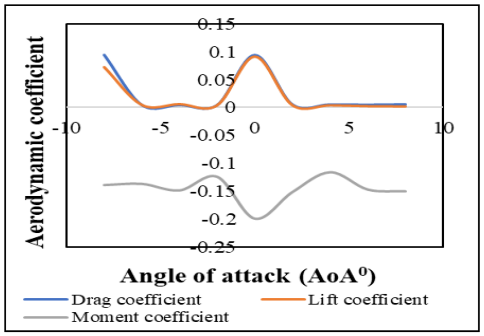

c) Sahara Desert region

Fig. 5. Variation of aerodynamic coefficients (Drag coefficient C_D, Lift coefficient C_L, Moment coefficient C_M) with angle of attack (AoA)

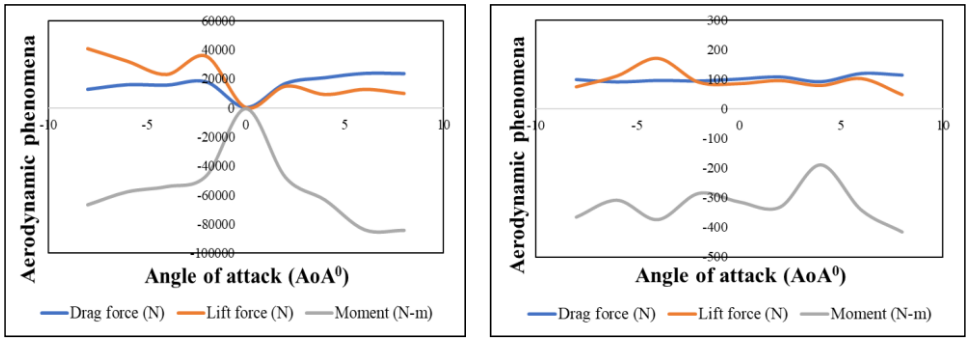

a) Katabatic wind-prone Antarctic region

b) Arctic Circle Region

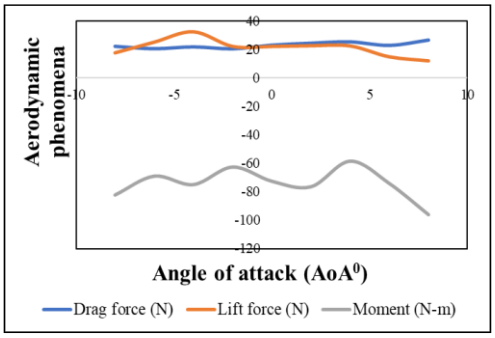

c) Sahara Desert Region

Fig. 6. Variation of aerodynamic forces (F_D, F_L, F_M) with angle of attack (AoA)

The coefficients of C_D, C_L, and C_M of 3 distinct climates are mentioned in Fig. 5, which indicates relatively steady values throughout the AoA, while the CM showed a notable and large deflection in 6°, 8°, and 0°, -8° in the Antarctic and Arctic regions, respectively. The Sahara Desert showed the least severe aerodynamic loading and more stable flow due to lower wind speeds and air density.

3.1 Pressure contour lines indicating the Eddy viscosity

The forces influenced by 3 distinct climates are mentioned in Fig. 6, indicating that the drag and lift forces of the Antarctic region are extremely high with values peaking around ±60,000 N, and the moment force shows strong nonlinearity, dropping to nearly -100,000 N·m at negative AoA. The Arctic region showed maximum lift and drag forces near ±300 N and moment forces below -500 N·m. while in the Sahara, the drag and lift are under ±40 N and moments near -120 N·m due to low wind speed and air density. The nonlinear moment behaviour of the deck in the Antarctic region at specific angles of attack (AoA) arises from complex flow separation and vortex shedding phenomena caused by the high-speed wind influenced by dense katabatic winds. At these AoA, strong turbulent eddies form and detach from the bridge deck surface, altering pressure distribution and generating fluctuating moments.

It has been observed that the integration of these parameters creates a large difference in response. The eddy viscosity indicates that the integration of high-density/low temperature wind and turbulence percentage along with other micro parameters generate a lot of thrust on the deck, which leads to vortex shedding and separation of the wind. Whereas the higher temperature/ lower density winds generate a low-intensity vortex and air separation. Additionally, the angle of attack has captured a lot of functionality in framing the effect of wind in Figs 7, 8, and 9.

The eddy viscosity contours indicate the amplified unsteady aerodynamic forces and cause the observed nonlinear moment response. This contrasts with the milder turbulence and steadier flow patterns in the Arctic and Sahara, leading to more linear moment behaviour. The comparison of Eddy viscosity in Figs. 7, 8, and 9 highlights the severe turbulence flow effect on the bridge deck in the Antarctic region, which results in larger and stronger eddies that can amplify unsteady aerodynamic forces and potentially compromise structural stability. On the other hand, the Arctic Circle faces moderate turbulence effects, and the Sahara experiences the least severe turbulence effect. This indicates that colder, denser air with higher wind speeds tends to intensify aerodynamic challenges. The contour colours [Pa s] are a clear indication of the intensity of viscosity.

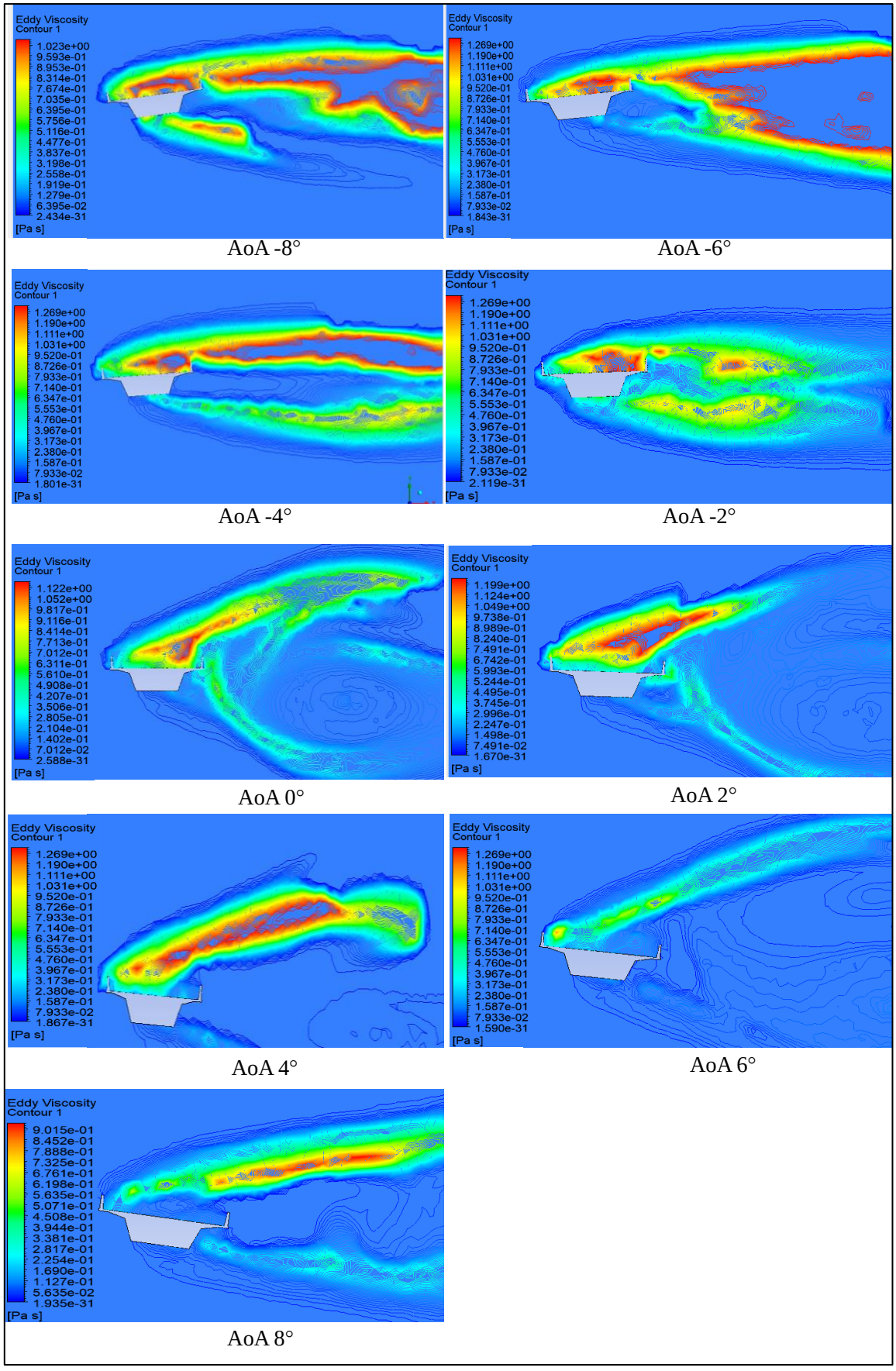

Fig. 7. Eddy viscosity contours under Antarctic, katabatic wind for the bridge deck.

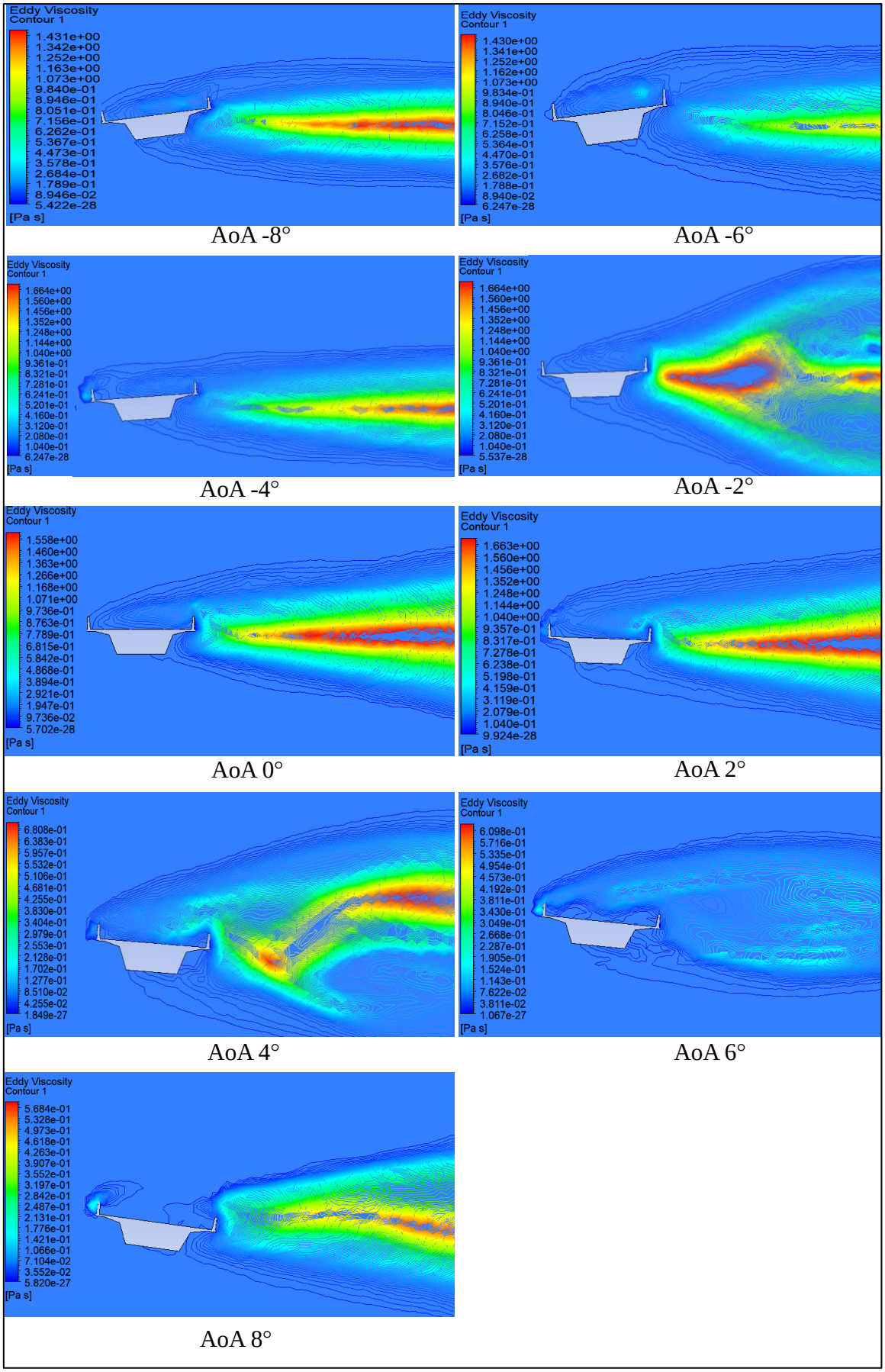

Fig. 8. Eddy viscosity contours under the Arctic Circle region for the bridge deck.

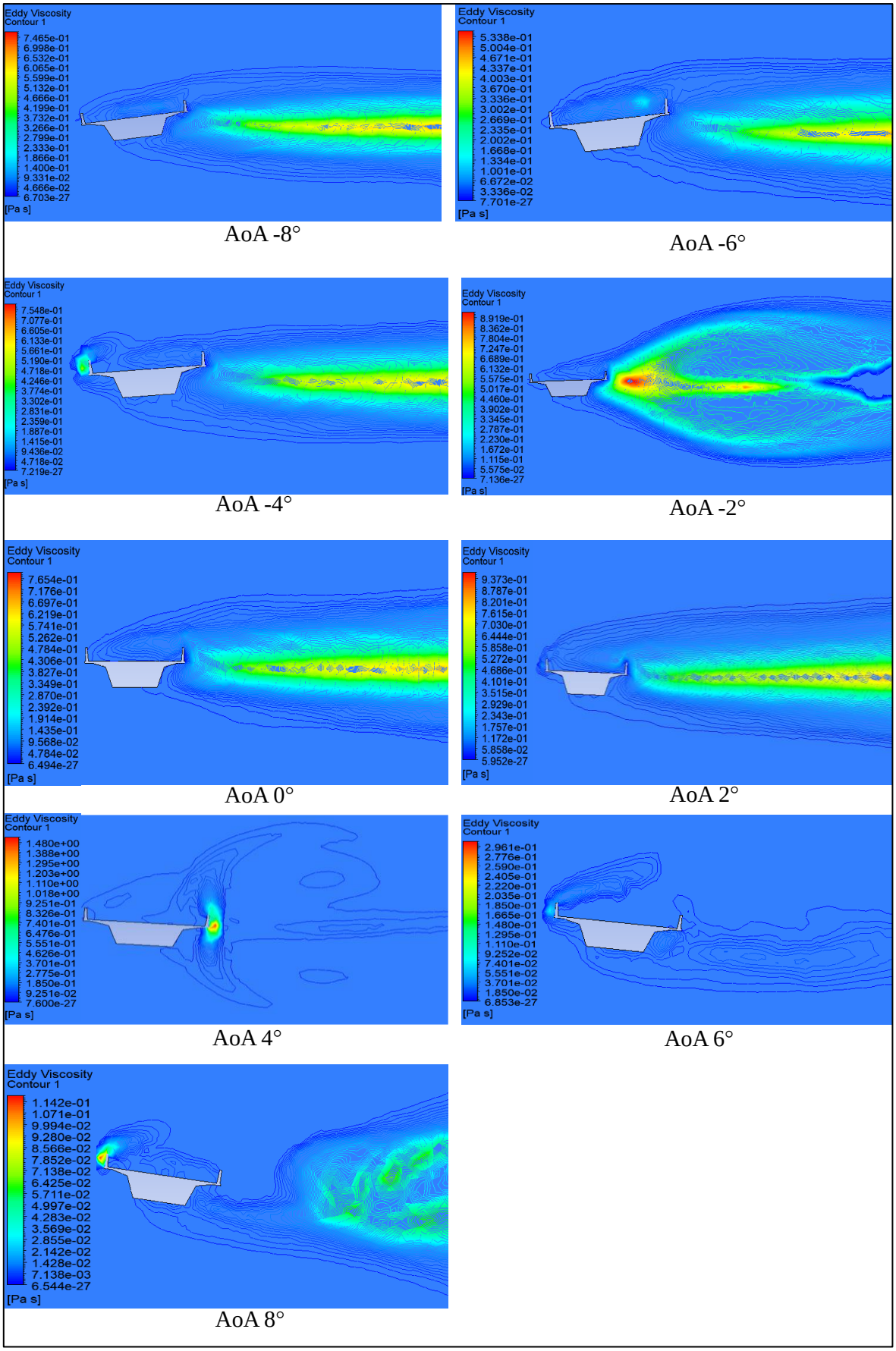

Fig. 9. Eddy viscosity contours under the Sahara Desert wind for the bridge deck.

4 Conclusion

The aerodynamic analysis across three regions shows that, while drag, lift, and mo-ment coefficients share similar trends with angle of attack, actual aerodynamic force magnitudes vary substantially due to environmental conditions. The katabatic wind-prone Antarctic region exhibits exceptionally high forces, far exceeding those in the Arctic Circle and the Sahara Desert. This highlights that relying solely on coefficients may mask critical design risks—full force calculations using local data are essential. Ultimately, robust region-specific assessment is necessary to prevent underestimating structural or stability hazards in extreme environments, especially for high-wind regions like the Antarctic. The result demonstrates that the katabatic winds of the Ant-arctic region impose the most critical aerodynamic forces on long-span bridge decks due to their high speeds, dense air, and intense turbulence. This indicates a vital role of including climatic parameters into bridge design to enhance safety and durability. Engineers should consider increased safety margins and adopt more conservative load factors when designing for such harsh environments. The current design requires a scrutiny to explicitly include region-specific aerodynamic loading parameters like those identified here, to prevent underestimating risks. Moreover, the selection of high-performance materials with superior fatigue resistance and durability against fluctuating wind loads is vital to ensure long-term structural integrity in these demanding conditions.

Acknowledgement

The authors sincerely acknowledge the valuable support and contributions of Mr Rohan Das from Indian Institute of Technology Bombay in conducting the aerodynamic analysis using ANSYS Fluent.

References

1. Y. L. Xu and W. H. Guo, ‘Dynamic analysis of coupled road vehicle and cable-stayed bridge systems under turbulent wind’, Eng Struct, vol. 25, no. 4, pp. 473–486, 2003, doi: 10.1016/S0141-0296(02)00188-8.

2. M. Cid Montoya, F. Nieto, S. Hernández, A. Fontán, J. A. Jurado, and A. Kareem, ‘Optimisation of bridges with short gap streamlined twin-box decks considering structural, flutter and buffeting performance’, Journal of Wind Engineering and Industrial Aerodynamics, vol. 208, Jan. 2021, doi: 10.1016/j.jweia.2020.104316.

3. A. Alonso-Estébanez, J. J. Del Coz Díaz, F. P. Álvarez Rabanal, and P. Pascual-Muñoz, ‘Numerical simulation of bus aerodynamics on several classes of bridge decks’, Engineering Applications of Computational Fluid Mechanics, vol. 11, no. 1, pp. 435–449, Jul. 2017, doi: 10.1080/19942060.2016.1201544.

4. Haldar, P., & Karmakar, S. (2024). Aerodynamic and flutter performance of the bridge deck with various countermeasures using computational fluid dynamics. Structure and Infrastructure Engineering, 1-19.

5. Haldar, P., & Karmakar, S. (2024). Aerodynamic and aeroelastic response of wind barrier over trapezoidal box girder bridge under turbulence wind. Indian Journal of Engineering & Materials Sciences, 31(2).

6. Miller, L. M., & Keith, D. W. (2018). Climatic impacts of wind power. Joule, 2(12), 2618-2632.

7. Li, S. H. (2023). Impact of climate change on wind energy across North America under climate change scenario RCP8. 5. Atmospheric Research, 288, 106722.

8. Haldar, P., & Karmakar, S. (2023). Wind response on RC trapezoidal box girder bridge using computational fluid dynamics. Sādhanā, 48(2), 74, doi: 10.1007/s12046-023-02127-xS.

9. A. Weber, H.-J. Bart, and A. Klar, 'Simulating Spiraling Bubble Movement in the EL Approach', Open Journal of Fluid Dynamics, vol. 07, no. 03, pp. 288–309, 2017, doi: 10.4236/ojfd.2017.73019.

10. Shih, T. H., Liou, W. W., Shabbir, A., Yang, Z., & Zhu, J. (1994). A new k-epsilon eddy viscosity model for high Reynolds number turbulent flows: Model development and validation (No. CMOTT-94-6).

11. T. Travouillon, M. C. B. Ashley, M. G. Burton, J. W. V. Storey, and R. F. Loewenstein, 'Atmospheric turbulence at the South Pole and its implications for astronomy', Astron Astrophys, vol. 400, no. 3, pp. 1163–1172, 2003, doi: 10.1051/0004-6361:20021814

12. B. J. Butterworth, G. de Boer, and D. Lawrence, 'A Study of Intermittent Turbulence in Stable Arctic Boundary Layers', Boundary Layer Meteorol, vol. 190, no. 1, Jan. 2024, doi: 10.1007/s10546-023-00847-5.

13. L. Garcia-Carreras et al., 'The turbulent structure and diurnal growth of the Saharan atmospheric boundary layer', J Atmos Sci, vol. 72, no. 2, pp. 693–713, 2015, doi: 10.1175/JAS-D-13-0384.1.